JOURNAL OF MATERIALS SCIENCE 10 (1975) 1137–1148

Kinetics of niobium carbide precipitation in a low carbon austenitic steel

S. J. HARRIS, N. R. NAG*
Department of Metallurgy and Materials Science, University of Nottingham, UK

An examination has been made of the kinetics of niobium carbide precipitation in a 18-10-1 austenitic stainless steel in the temperature range 650 to 750° C. Electrical resistance-time plots, thin film electron microscopy and hardness measurements have been employed to follow the ageing sequence. In these alloys the carbides precipitate on undissociated dislocations and in association with stacking faults; these processes are diffusion controlled and have an activation energy of ~ 318 kJ mol^{-1}. Prior to the reaction beginning a clear incubation period existed, e.g. ~ 30 h at 650° C and 20 min at 750° C. During the first 10% transformation the carbide nucleation rate increases and the associated faults nucleate and grow rapidly. The carbide nucleation rate appears to peak around this level and then falls away gradually to zero around 70% transformation. At this latter stage fault growth ceases, and transformation continues by a carbide growth process. The age-hardening peak occurs much beyond the end of the reaction by which time precipitate coarsening is in evidence. The precise effect mechanical deformation has upon stacking fault formation depends to a major extent on the niobium supersaturation in the quenched alloy.

1. Introduction

Austenitic steels with better mechanical and corrosion resistant properties can be obtained by making small additions of elements such as titanium, niobium and vanadium. These elements form stable compounds with the small residual amounts of nitrogen and carbon in these steels. Carbide and nitrides can nucleate and grow, (a) homogeneously in the matrix, (b) on undissociated dislocations and, (c) in association with stacking faults.

Numerous observations [1-4] have been made using thin film electron microscopy to elucidate the morphology of such precipitates on dislocations and stacking faults. The results allowed Hirsch [2] and Silcock and Tunstall [3] to suggest mechanisms by which stacking-fault precipitation occurred in these alloys. The nucleation of the fault takes place when a dislocation loop is thrown off from a carbide (or nitride) particle which has formed on an undissociated dislocation. As the loop dissociates, more carbide precipitates nucleate on the outer partial of the resultant fault, i.e. on the Frank partial. For continued growth of these precipitates, a supply of vacancies would be necessary to relieve the transformation strains, instead the Frank partial climbs providing vacancies for the nucleation of more precipitates.

Attempts have been made to study the kinetics of the stacking-fault reaction by dilatometry [5], electrical resistance [6], hardness [7] and quantitative microscopy [8] techniques, in each case differences have arisen with respect to each other and with respect to the mechanisms outlined above. Barford *et al.* [6] has shown that an increase in electrical resistance takes place in the early stages of ageing, and this was explained in terms of a "short-range ordering process'. Dilatometry data [5] showed no sign of this kind of process, only a conventional incubation process, but analysis of the sigmoidal transformation curves indicated that growth of stacking faults is complete after only 10% of the niobium carbide has been precipitated, the remaining 90% of the reaction being a diffusional growth process. The quantitative measurements made on electron micrographs of stacking-fault diameter [8, 9] tend to indicate that the growth of faults occurs for much longer periods

*Present address: British Steel Corporation (Strip Mills Division) Port Talbot, UK.

and, therefore, seems to be at variance with the interpretation afforded by the data from the physical measurement techniques. Harding and Honeycombe [7] showed that the hardness-time plots gave an indication of maximum hardness occurring a long time after fault growth had ceased.

The effects of different quenching rates [8, 9], deformation [1] and supersaturation of carbide forming elements [10, 11] on the growth of faults has been assessed by electron microscope observations. However, no attempt has been made to assess these process variables on the overall reaction kinetics of the process.

In the present work, attempts have been made to correlate precipitation morphology, fault growth and mechanical properties with the overall kinetics of reaction in a nickel-chromium austenite with niobium present. The effect of plastic deformation immediately prior to ageing also has been assessed in all these respects.

2. Experimental

The materials used in this work were commercially manufactured nickel-chromium-niobium austenite steels, and were supplied by Firth Vickers Ltd, as 16 mm diameter bars. The chemical analyses of the steels are given in Table I.

Kinetics of the precipitation processes have been determined by making electrical resistance measurements on 216 mm long pieces of bar at the ageing temperature. The temperature along the bar was maintained within $\pm$ 1°C for periods of up to 20 days in a furnace tube pumped continuously to a vacuum of $\sim 10^{-5}$ Torr. Prior to the ageing sequence, specimens were solution treated at 1300°C in a vacuum furnace and then quenched in a 10% brine solution. After inserting the quenched bar into the ageing furnace, a period of 2 to 3 h was required for temperature equilization. A Kelvin double bridge was used to measure the electrical resistance at regular intervals of time, allowing changes in resistance to be plotted against time of ageing. For the series of experiments involving plastic deformation prior to ageing a dead weight load was applied to the specimen by linking it to the loading mechanism of a modified creep machine. The amount of deformation was measured as the percentage elongation of the sample.

Electron microscopy has been carried out on samples thinned from those used for electrical resistance measurements or from pieces of bar, 50 mm long, that have been aged in similar circumstances. Discs $\sim$ 2 mm thick were cut from the samples, and both faces were initially abraded on a lapping machine to $\sim$ 0.2 mm thickness. Final preparation was by an electropolishing technique using an acetic-perchloric acid mixture (95:5) at a voltage of 39 V, temperature 15 to 20°C.

Hardness measurements were made at various points across the cross-section of the bar using a 10 kg load.

3. Results

3.1. Electrical resistance changes – straight ageing

Ageing curves were plotted from the data provided by the changes in electrical resistance which occurred as a function of time, i.e. $(R_t - R_0/R_0) \times 100$ versus log t; where R_t and R_0 are the resistances at any time t and at zero time. The curves obtained at 650, 675, 700, 725 and 750°C were normalized and are shown in this form in Fig. 1. At 650 and 675°C, the ageing process was stopped after 7 days, i.e. before transformation was complete; to allow normalization of data it was assumed that the total resistance change at the end of the process was the same as that which occurred at 725°C. All the curves were sigmoidal in shape and had an incubation period during which no change in resistance took place. It can be seen that the incubation period increases by two orders of magnitude as the temperature falls by 100°C.

The Johnson-Mehl equation [12] was used to analyse the transformation curves:

$$y = 1 - \exp - (kt)^n \qquad (1)$$

where y is the fraction precipitated, t the time and k and n are constants. The values of the time exponent n can be used [13] to interpret the kinetics of the reaction. To determine n, plots were made of log log $1/(1 - y)$ versus log t, for each ageing curve (see Fig. 2). It was found that discontinuities existed in each plot, i.e. no continuous straight line could be drawnthrough the points. Whilst this kind of behaviour is usual at 0.95 fraction transformed, i.e. when overlapping diffusion fields exist [14], here deviations were found to exist at most temperatures in the neighbourhood of 0.1 and 0.7 fraction transformed. Table II gives the values obtained from measuring the slopes of the lines in Fig. 2. At

TABLE I Chemical analysis of steel

	Element (wt%)												
Steel no.	C	Si	Mn	S	P	Ni	Cr	Mo	V	Cu	Ti	Nb	N
A	0.02	0.36	1.21	0.008	0.012	12.50	18.50	0.07	0.08	0.08	0.06	0.94	0.025
B	0.05	0.54	0.83	0.011	0.015	9.50	17.10	0.10	0.03	0.10	0.01	0.71	0.027

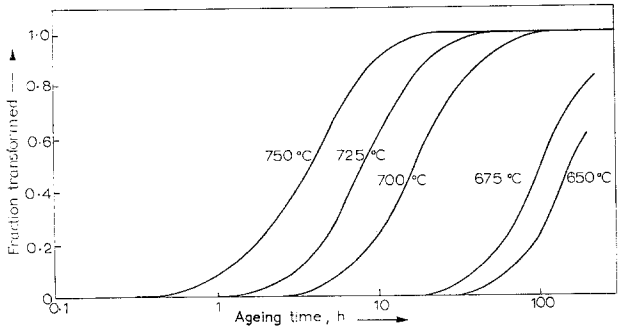

Figure 1 Normalized ageing curves obtained from variations in electrical resistance measured with respect to time.

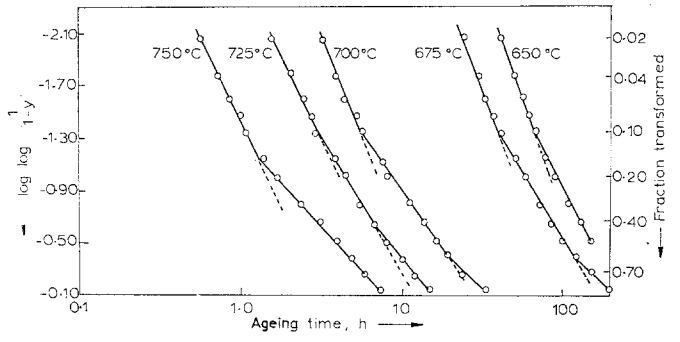

Figure 2 Plots of log log $1/(1 - y)$ against log t showing discontinuities at certain stages of transformation.

TABLE II Johnson-Mehl time exponent, n, at different stages of transformation

Temperature (°C)	Time exponent, n		
	$y < 0.1$	$y > 0.1$ < 0.7	$y > 0.7$
650	3.3	2	—
675	3.3	1.9	—
700	3.0	2.1	1.1
725	2.6	1.95	0.9
750	2.6	1.2	1.1

750°C, a single change took place at $\sim$ 0.1 fraction transformed.

The activation energy for the precipitation reaction was determined at $y = 0.1$ and 0.5 using Arrhenious type plots (see Fig. 3). Values of $\sim$ 318 kJ mol^{-1} was obtained in both cases.

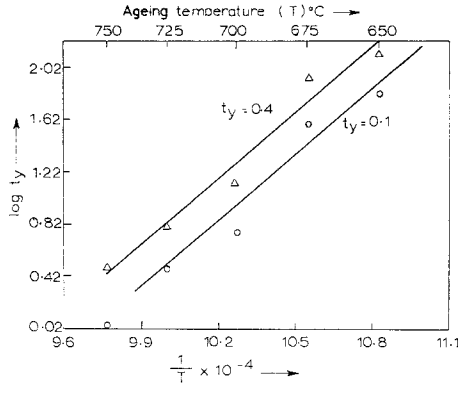

Figure 3 Arrhenius plots for determining the activation energy for the precipitation reaction at two levels of transformation.

3.2. The effect of prior deformation on electrical resistances curves

Deformations in the range 2 to 6% were applied to samples at the ageing temperature, immediately resistance measurements were begun and continued until no further change in this property took place (see Fig. 4a and b). It was noted in samples that had received between 4

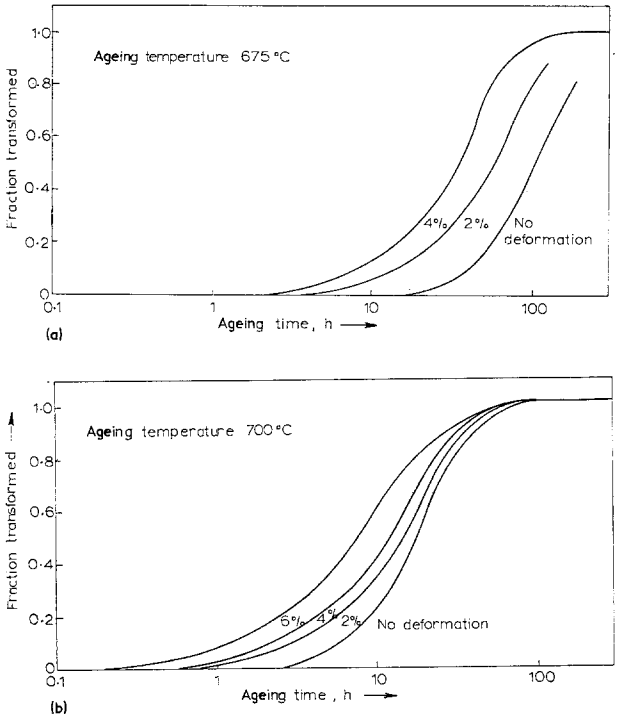

Figure 4 Effect of prior deformation on the ageing curves (a) at 675° C, (b) at 700° C.

and 6% deformation, that the incubation period was shortened by one order of magnitude, whilst the end point of the process was reduced by never more than one half.

Determination of n from log log $1/(1 - y)$ versus log t plots indicated that a change in this parameter occurred in the neighbourhood of $y = 0.1$. Much lower values were obtained for $y < 0.1$ and an increase took place once this level of transformation had passed, see Table III.

TABLE III The effect of deformation on the Johnson-Mehl time exponent, n

Temperature (°C)	% Deformation	Time exponent, n	
		$y < 0.1$	$y > 0.1$
675	2	0.6	1.7
	4	0.95	1.4
700	2	0.95	1.3
	4	0.9	1.3
	6	1.1	1.2

3.3. Hardness measurements

These measurements were made on a series of samples aged at 700° C, they are shown in Fig. 5. A rise of 100 HV took place as a result of the ageing process. For comparison the electrical resistance-time curve is plotted in Fig. 5 and it can be seen that the precipitation reaction is complete before the hardening peak is reached.

3.4. Thin film electron microscopy

3.4.1. Effect of temperature on precipitate morphology

Examination of thin foils prepared from samples used for electrical resistance measurements indicated that at all ageing temperatures, precipitation of niobium carbide occurred on both undissociated dislocations and in association with stacking faults (Fig. 6a). It was noted at 750° C (Fig. 6b) that coarser carbide precipitates existed on undissociated dislocation than those existing in samples aged at lower temperatures.

3.4.2. Stages of precipitation during ageing at 700° C

These stages are shown in Fig. 7a to d. After 6 h (~ 0.1 fraction transformed) most of the dislocations were decorated with precipitates and stacking faults had begun to nucleate. From 6 to 40 h the stacking faults increase in number and size. Up to the 15 h stage (~ 0.4 transformation),

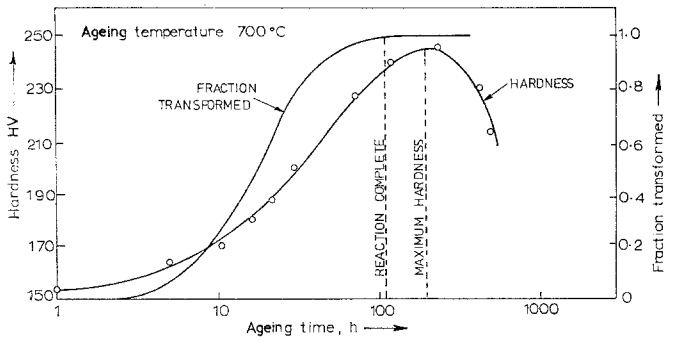

Figure 5 Hardness-log t plots for isothermal ageing at 700°C. For comparison, the appropriate electrical resistance curve is inserted.

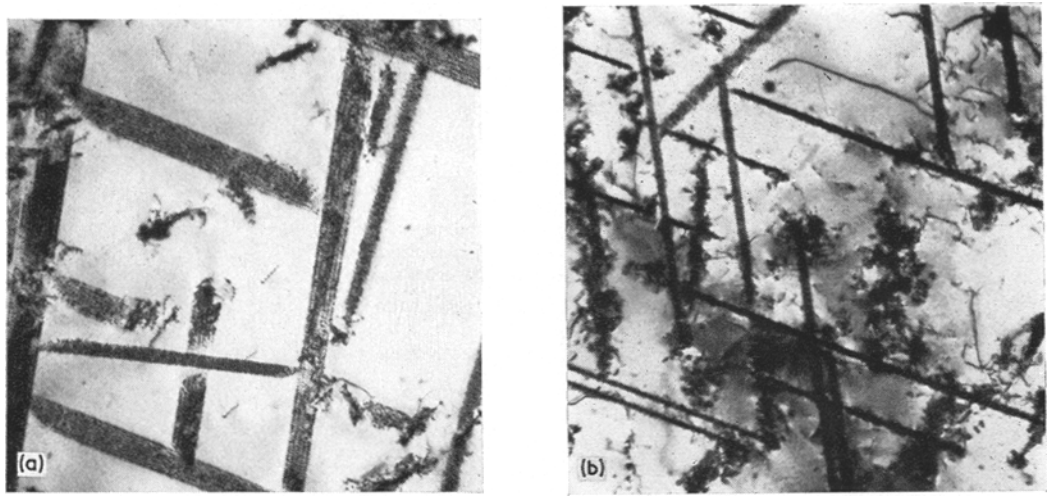

Figure 6 Thin foil electron micrographs showing the effect of temperature on the morphology of niobium carbide precipitates, (a) aged 100 h at 700°C, × 40 000; (b) aged 25 h at 750°C, × 20 000.

faults only showed fringe contrasts, but no particles were visible, whilst selected-area diffraction patterns showed matrix spots only. The first visual appearance of particles of niobium carbide occurred after 22 h (~ 0.6 transformation). No further increase in fault size could be detected beyond 40 h, but further ageing up to 130 h resulted in coarsening of precipitates within the faults and on undissociated dislocations (Fig. 7c). Electron diffraction patterns which could be indexed as niobium carbide began to appear in these latter stages of ageing (Fig. 7d).

3.4.3. Stages of precipitation during ageing at 675°C

Particular attention was given to the beginning of the reaction since the electrical resistance data indicated a long incubation period of 20 h at this temperature. Micrographs (Fig. 8a) taken at the 5 h stage showed no sign of precipitation and the undissociated dislocations appeared to exist in similar configurations to those found in the as-quenched material. Decoration of these same dislocations had begun by the 20 h stage, but still no stacking faults were observed. At 40 h (~ 0.1 fraction transformed) it was noted that each stacking fault had formed in association with a single undissociated dislocation decorated with precipitates (Fig. 8b). The original dislocation seemed to cross the fault indicating that it was possible that the undissociated dislocations and the stacking faults were in two different planes.

3.4.4. Effect of deformation on the ageing process

No stacking faults were observed in the samples which were deformed by > 6% and then subsequently aged at 675 and 700°C respectively, whilst after 2 and 4% deformation, increases in

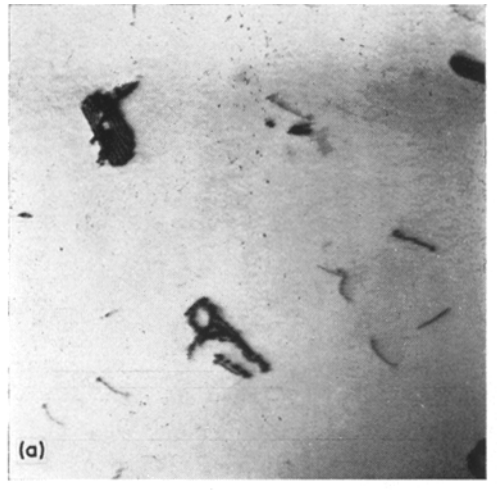

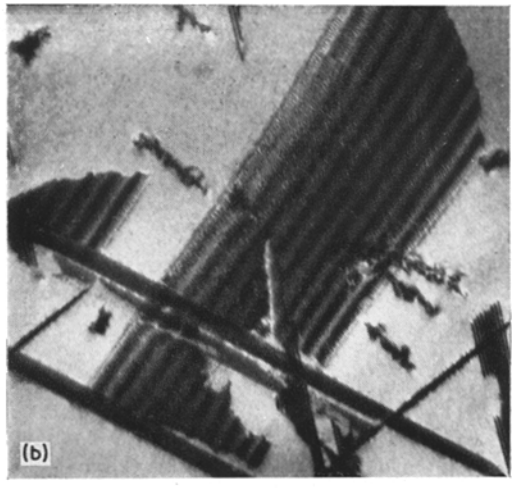

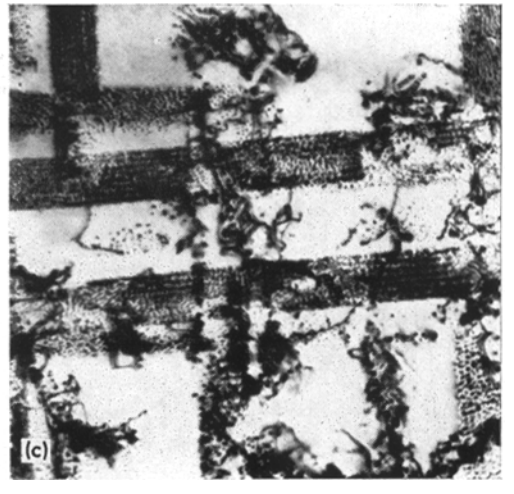

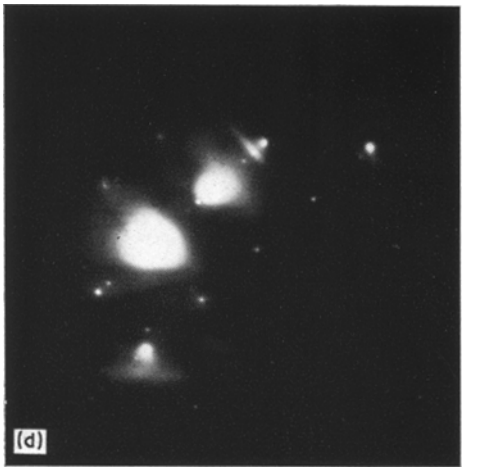

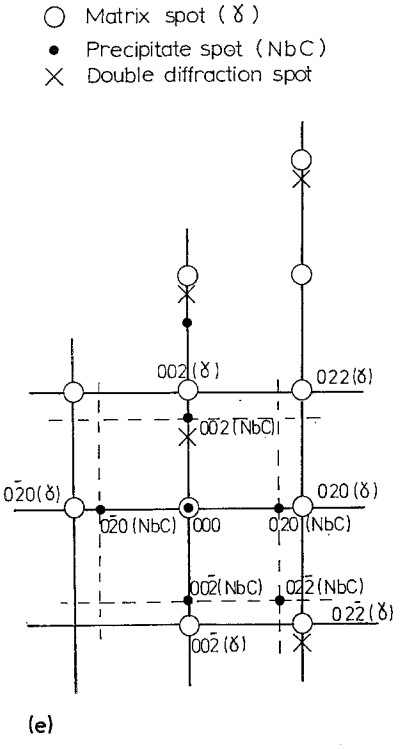

Figure 7 Transmission electron micrographs and diffraction patterns obtained on alloy B aged at 700°C for the following times: (a) 6 h, × 40 000, (b) 40 h, × 20 000, foil orientation {211}, (c) 130 h, × 60 000, foil orientation {100}, (d) selected-area diffraction of (c). (e) Diffraction pattern of (d).

the number of stacking faults were observed at both ageing temperatures. At higher deformations where stacking faults were not observed, more extensive growths of niobium carbide occurred on the dislocations present. Another

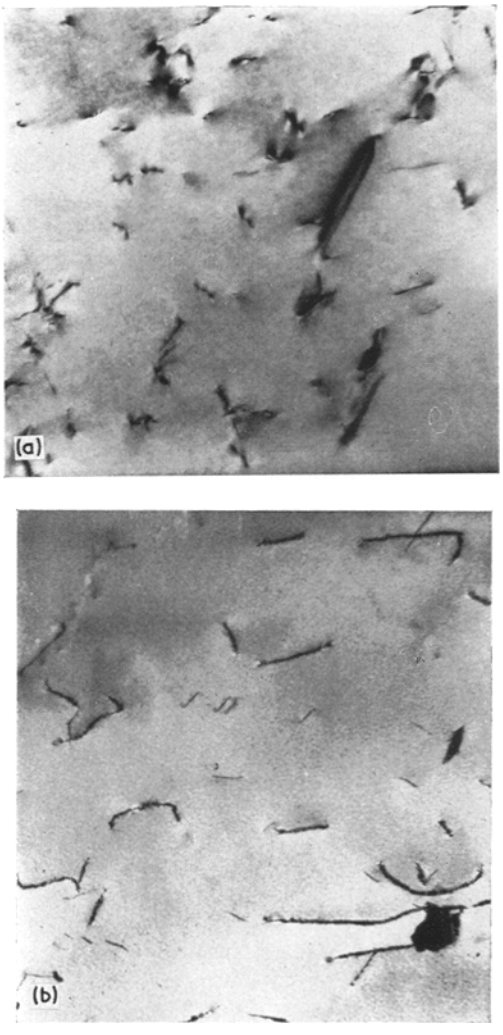

Figure 8 Transmission electron micrographs of alloy B aged at 675°C for (a) 5 h, × 20 000; (b) 40 h, × 20 000.

feature observed in the lightly deformed samples is that the incidence of stacking-fault precipitation is very much dependent on dislocation density in the matrix. Grains with higher dislocation densities showed very little evidence of faults whilst in a neighbouring grain, where the dislocation content is smaller, the faults are present in abundance (Fig. 9a to c).

3.5. Quantitative measurements on electron micrographs

In order to correlate more precisely the electrical resistance data with nucleation and growth of stacking faults and the associated niobium carbide precipitates, measurements (for details see Appendix I) have been made of stacking-fault diameter on a series of faults which have been prepared from samples aged at 700°C for various times (Fig. 10). The mean diameter increases smoothly with ageing time from 6 to 20 h; about this level the rate falls off slowly until a relatively constant mean value is reached in the neighbourhood of 30 h. It must be pointed out that a large scatter exists on the diameters measured in these latter stages of fault growth as the number of complete faults appearing on the micrographs was small.

Stacking-fault diameters were measured on materials which had been deformed prior to ageing. These samples showed that at a given amount of transformation, the diameter decreased with increased deformation, i.e. with increasing dislocation density, provided a certain amount of deformation had not been exceeded. Having received between 4 and 6% deformation and aged at 675 and 700°C, samples ceased to show stacking faults and precipitation only took place on undissociated dislocations. A count of the number of stacking faults and an assessment of dislocation density showed that there is an optimum dislocation density for which the number of faults passes through a maximum value.

4. Discussion

The precise kinetics of the nucleation and growth of niobium carbide precipitates in these materials are complex, particularly when associated with stacking-fault formation. When the Johnson-Mehl equation is used to assess the electrical resistance-time plots, it is apparent that several values of the time exponent n can be obtained at different stages of the transformation. The values of n may be interpreted according to Table IV.

For the purpose of this discussion, it is useful to divide the process into four stages, i.e. 0 to 0.1, 0.1 to 0.7, 0.7 to 1.0 fraction transformed, and overageing beyond full transformation. None of these divisions is intended to be set up as a precise boundary for explaining the kinetics but to give an indication of the stages at which changes are about to take place.

4.1. 0 to 0.1 fraction transformed

At this stage of the transformation, the n values decreased reasonably consistently from 3.3 at 650°C to 2.6 at 750°C (see Table II). These values are all in excess of 2.5 and, therefore, indicate that particles are being formed with an

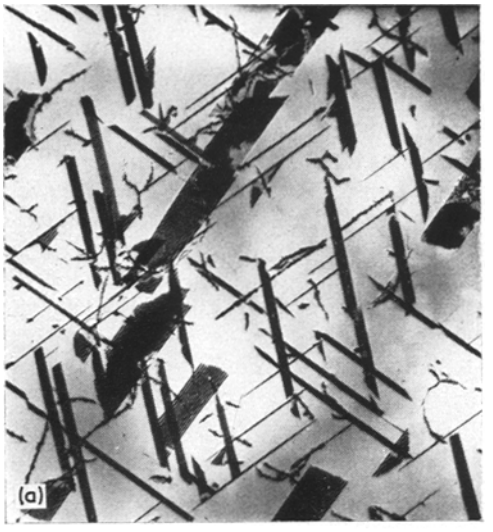

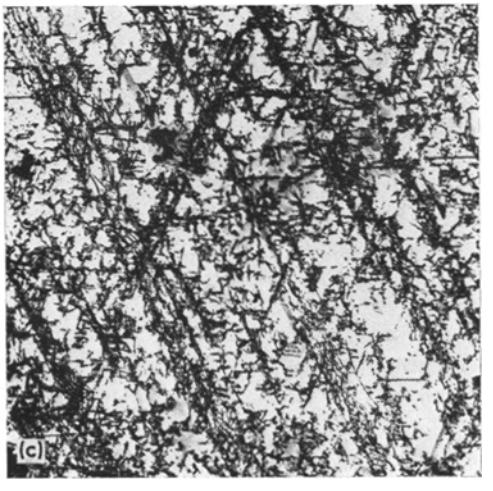

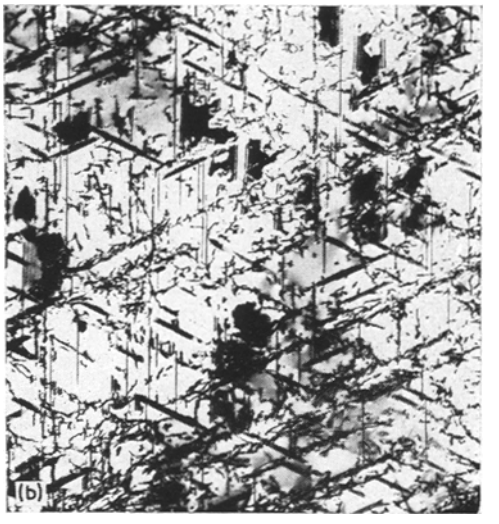

Figure 9 Thin foil electron micrographs showing the variation of the number of stacking faults with dislocation density in steel B which has been aged at 700°C for 40 h, (a) no deformation, × 8000; (b) 3% deformation, × 8000, area with low dislocation density, (c) as (b) except it is an area with high dislocation density. Foil orientation in all cases {211}.

increasing nucleation rate. There is clear evidence from the electron microscopic observation that precipitates nucleate on undissociated dislocations and then stacking faults begin to form at all ageing temperatures. This kind of evidence fits in well with the mechanism put forward by Silcock and Tunstall [3], i.e. the carbide nucleation sites rapidly increase with the advent of stacking-fault nucleation and growth. In such circumstances, the precipitates do not grow quickly once the climbing Frank partial moves on, hence the nucleation process dominates the kinetics. Such an interpretation is in keeping with the slightly lower n values found in the reaction at higher ageing temperatures, e.g. at 725 and 750°C, where an increased number of undissociated dislocations are decorated by precipitates without stacking faults being produced, thus reducing the density of faults. At these higher ageing temperatures, the combination of a smaller supersaturation of niobium and carbon and an increased vacancy concentration could reduce the effective driving force for carbide nucleation, allowing growth of the existing precipitates on undissociated dislocations to take place. From the measurements of stacking fault diameters, it is apparent that very small faults are present at 0.1 fraction transformed and above, showing that new faults are still being formed beyond this stage of ageing at 700°C and at lower temperatures.

4.2. 0.1 to 0.7 fraction transformed

Here the exponent n falls to values in the range 1.9 to 2.1 for ageing temperatures in the range 650 to 725°C. The interpretation of n values lying in the range 1.5 to 2.5 in such reactions is of diffusional growth with a decreasing nucleation rate. This would imply that the nucleation rate will increase rapidly up to $\sim$ 0.1 fraction transformed and then decay within the range 0.1 to 0.7. Again, electron microscopy backs up this interpretation and provides further information. At 700°C, small faults were still observed after 11 h ageing ($\sim$ 0.3 transformed) which would indicate that new stacking faults still can

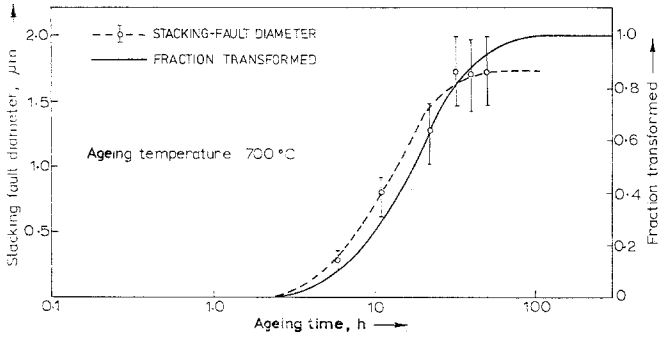

Figure 10 Variation of mean stacking-fault disc diameter with ageing time for alloy B at 700° C. The error bars give 95% confidence limits.

TABLE IV Interpretation of values of Johnson-Mehl exponent n for diffusion controlled process [13]

Conditions	n
All shapes growing from small dimensions, increasing nucleation rate	> 2.5
All shapes growing from small dimensions, constant nucleation rate	2.5
All shapes growing from small dimensions, decreasing nucleation rate	1.5–2.5
All shapes growing from small dimensions, zero nucleation rate	1.5
Growth of particles of appreciable initial volume	1–1.5
Precipitation on dislocations (very early stages)	0.5

be formed at this stage. However, as the plot in Fig. 10 indicates, the incidence of new faults at this time must be small. Between 0.1 and 0.3 fraction transformed, the diameters of the majority of faults have begun to increase rapidly, thus confirming the quantitative electron microscope results of Silcock *et al.* [9] in the early stages of ageing at 700° C. After 22 h ageing (~ 0.6 transformed), the rate of increase of the diameter has tended to slow down, although almost all the faults have grown above the maximum diameter measured at 11 h; appreciable reduction in the rate of fault growth has occurred at 31 h (~ 0.8 transformed). Hence, the decaying nucleation rate which is in evidence from the Johnson-Mehl analysis may be interpreted as a gradual reduction and a final cessation of new stacking-fault production, followed by a slow reduction in fault growth rates which, in turn, means a gradual reduction in effective carbide nucleation rates as the Frank partials climb more slowly. There is clear evidence here that fault growth still occurs up to 0.7 fraction transformed which is considerably in excess of the value of 0.2 which had been previously stated with dilatametric studies [5].

The results obtained on the samples aged at 750° C have been left out of the discussion to date because beyond ~ 0.1 transformed an abrupt change in the value of n takes place from 2.6 to 1.2. The lower values can be interpreted in terms of a straightforward diffusional growth process with zero nucleation rate. Examination of the electron micrographs of samples aged at this temperature indicates that precipitates occur on undissociated dislocations and that stacking-fault growth has taken place. However, two principal observations were made:

(i) the density of stacking faults was reduced;

(ii) the carbide precipitates on undissociated dislocations and on stacking faults was much coarser than had been observed at lower ageing temperatures.

This would indicate that the niobium carbide nucleation rate on undissociated dislocations and on Frank partials had rapidly decayed.

4.3. 0.7 to 1.0 fraction transformed

Beyond 0.7 fraction transformation, the n value decreases in cases where values could be obtained (700, 725 and 750° C) to 0.9 to 1.1. Such values point to diffusion growth at zero nucleation rates. Support for this view is found from the trends shown by the stacking faults mean diameter measurements that cease to increase beyond ~ 0.7 transformation (Fig. 10). These results tend to indicate that fault growth rapidly decreases because carbide nucleation is at an end. Beyond this stage transformation continues to completion entirely by carbide growth. In experiments carried out to determine the effect of supersaturation of niobium on the precipitation of niobium carbide it has been shown that the

minimum solute content for stacking fault formation is $\sim 0.25\%$ Nb [11]. In the present investigation, the amount of niobium which still remained in solution after 0.7 transformation was 0.27%. Both pieces of evidence reinforce the concept that stacking faults will not grow beyond a given limit which can be either specified in terms of supersaturation or the fraction transformed in a given alloy.

4.4. Beyond full transformation

It was noted that the hardness values continued to increase with ageing time beyond the end of the reaction as designated by the flattening out of the sigmoidal resistance-time curve. Fig. 5 shows that such a maximum occurs after 200 h ageing at 700°C, which is almost twice the time at which the electrical resistance remains constant. If the resistance measurements are accepted as defining the end of the carbide reaction, the rise in hardness could be explained by a coarsening process which does not involve an increase in the precipitate volume fraction. Clear electron microscopic evidence of carbide coarsening at 130 h ageing at 700°C is shown in Fig. 7c.

4.5. Effect of deformation prior to ageing

At both ageing temperatures, 675 and 700°C, deformation consistently reduced the incubation period for the transformation, this is particularly shown by the resistance measurements, e.g. the period is reduced by one order of magnitude by 4% deformation applied immediately prior to ageing at 675°C. In the stage 0 to 0.1 fraction transformed, the exponent n has a low value, i.e. in the range 0.9 to 1.0, in comparison with values of ~ 3.3 for the ageing-only procedure. The electron microscope helps show substantial increases in the density of undissociated dislocations in those specimens without any stacking faults being observed. Above 0.1 transformation, n increases to values in the range 1.2 to 1.7. It was noted that the transformation fraction where this change takes place increases with increasing deformation. An interpretation of this experimental evidence is that niobium carbide nucleates on the increased undissociated dislocation population in these early stages, the number of nuclei increasing with prior deformation. Diffusional growth of the carbides may be enhanced at this early stage because the deformation could have increased vacancy concentrations in the matrix permitting larger precipitates to be accommodated. All these precipitates are nucleated within a short period and after this, growth proceeds with effectively a zero nucleation rate, hence the value of n close to 1.0. The heavier the deformation, the larger the vacancy concentration, the longer the growth process can proceed on a greater number of carbide precipitates on a higher dislocation density without stacking-fault growth being involved. Supporting evidence for this statement is given in Fig. 9, which shows stacking faults occurring in a grain of low dislocation density whilst none form in one of high dislocation density.

The n values increase appreciably above 1.0 as the reaction proceeds, thus gives an indication of stacking-fault formation, i.e. nucleation of carbide particles begins to occur again as the Frank partial climbs. In this case, a very large number of faults may begin to grow but they may only grow to a limited size (Fig. 9b). A stage will be reached where the undissociated dislocation density will be sufficient, e.g. in a sample given 6% deformation at 700°C, where the n value changes very little throughout the reaction and no evidence can be found of stacking faults. Here the transformation has proceeded using the undissociated dislocations for carbide nucleation and growth to a stage where the supersaturation of niobium has been reduced to below $\sim 0.25\%$ and stacking-fault growth does not even begin. Intermediate situations exist, e.g. between 4 and 6% deformation at 700°C, where maximum fault densities form due to the increased undissociated dislocation density being capable of forming faults, i.e. the matrix is still just sufficiently saturated in Nb.

4.6. General comments

From all these observations, it is concluded that stacking-fault precipitation depends on three principal factors which are obviously interrelated to each other:

(1) dislocation density;
(2) supersaturation of solute atoms;
(3) concentration of vacancies.

Out of these, the dislocation density is the main controlling factor since the initial precipitate on an undissociated dislocation is an essential requirement for the nucleation of a stacking fault. Supersaturation is a governing factor in the sense that after saturating these initial sites, the majority of the precipitation process will take place in concert with stacking-fault growth. A high supersaturation is necessary for this type of

precipitation if large dislocation contents are present. The role of vacancy concentration is more difficult to tie down, for it would appear to control the growth and, therefore, the size of the precipitates on original dislocations before they throw out climb loops for providing more vacancies. Whether the effect of delaying the initiation of faults is greater than the increase in the diffusivity of solute atoms which may reduce the time for attaining the critical size for throwing out loops, is open to debate.

5. Conclusions

(1) The precipitation of carbides on stacking faults and undissociated dislocations is diffusion controlled and has an activation energy of ~ 318 kJ mol^{-1}.

(2) Electrical resistance and quantitative microscopy measurements indicate that an increasing carbide nucleation rate exists for the first 10% of transformation, during which stage stacking faults initiate and rapidly grow.

(3) Beyond 10% transformation, carbide nucleation rate decreases reaching zero close to 70% transformation. This is accompanied by a reduction in fault nucleation and a slowing down of fault growth.

(4) Beyond 70% transformation and up to reaction completion, carbides grow whilst fault size and number remains essentially constant.

(5) Coarsening of carbides takes place after the reaction is complete and the age-hardening peak is achieved during this stage.

(6) A relationship exists between the dislocation density which may be introduced by prior deformation and the degree of supersaturation of niobium in the quenched alloy, for if the supersaturation is below a certain level, faults will never form and grow.

Appendix. Method used for the measurement of stacking-fault diameter

Fig. 11 shows the section of a stacking fault which is cut by the top and bottom of a foil of thickness t. The foil plane is represented by ABCD and PQ and RS are the lines of intersection of the stacking-fault plane with the top and bottom of the foil. θ is the angle of inclination between the stacking-fault plane and the foil plane, l_1 and l_2 are the lengths of the two parallel sides and b is the projected breadth of the fault. If one considers the faults are circular in shape then PQRS can be represented as a segment of the completed stacking-fault as

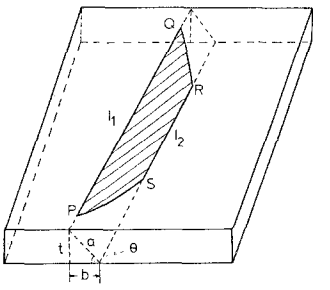

Figure 11 Construction showing the position of the stacking fault in the thin foil.

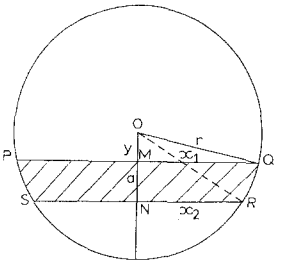

Figure 12 Segment PQRS shown as being part of a complete circular fault shape.

shown in Fig. 12. If r is the radius of the fault then,

$$r^2 = x_1^2 + y^2 \tag{2}$$

$$r^2 = x_2^2 + (y + a)^2 . \tag{3}$$

Equating Equations 2 and 3

$$x_1^2 + y^2 = x_2^2 + y^2 + a^2 + 2ya$$

$$y = \frac{x_1^2 - x_2^2 - a^2}{2a} .$$

Putting the value of y into Equation 2

$$r^2 = x_1^2 + \frac{(x_1^2 - x_2^2 - a^2)^2}{2a} .$$

From Fig. 11, $a = b/\cos\theta$,

$$\therefore r^2 = x_1^2 + \left[\frac{x_1^2 - x_2^2 - (b/\cos\theta)^2}{2b/\cos\theta}\right]^2 . \tag{4}$$

Again from Figs. 11 and 12,

$$x_1 = \frac{l_1}{2}$$

and

$$x_2 = \frac{l_2}{2} .$$

Therefore, Equation 4 can be written as,

$$r^2 = \frac{l_1^2}{4} + \left[\frac{(l_1^2/4) - (l_2^2/4) - (b/\cos\theta)^2}{2b/\cos\theta}\right]^2 \quad (5)$$

The values of l_1, l_2 and b for each stacking fault can be measured from micrographs and, if θ is known, the actual diameter ($2r$) of the fault can be calculated using Equation 5.

In the present case, measurements have been carried out on micrographs taken at {100} foil orientation. At this orientation of the foil, all four {111} planes have an inclination of 54°74′ to the foil plane. As the fault planes are {111}, each fault which appeared on the micrograph has a similar angle of inclination, i.e. 54°74′ to the foil plane.

Acknowledgements

The authors would like to extend their thanks to Dr B. Noble for helpful guidance on the electron microscopic aspects of this work. One of the authors (NRN) is grateful to the Ministry of Defence for providing a research grant whilst this programme was carried out. Also our thanks are extended to Professor J. S. L. Leach for the provision of laboratory facilities.

References

1. J. S. T. VAN ASWEGAN, R. W. K. HONEYCOMBE and D. H. WARRINGTON, *Acta Met.* **12** (1964) 1.
2. P. B. HIRSCH, *N.P.L. Conference* **1** (1963) 440.
3. J. M. SILCOCK and W. T. TUNSTALL, *Phil. Mag.* **10** (1964) 361.
4. J. J. IRANI and R. T. WEINER, *J. Iron Steel Institute* **203** (1965) 913.
5. J. BARFORD, *ibid* **204** (1966) 134.
6. J. BARFORD, M. J. KNIGHT and J. M. SILCOCK, *ibid* **204** (1966) 122.
7. H. J. HARDING and R. W. K. HONEYCOMBE, *ibid* **204** (1966) 259.
8. D. W. BORLAND and R. W. K. HONEYCOMBE, *Met. Sci. J.* **4** (1970) 14.
9. J. M. SILCOCK, K. W. SIDDING and T. K. FRY, *ibid* **4** (1970) 29.
10. M. C. CHATURVEDI, R. W. K. HONEYCOMBE and D. H. WARRINGTON, *J. Iron Steel Institute* **206** (1968) 1236.
11. J. M. SILCOCK and A. W. DENHAM, Symposium on "Mechanism of phase transformation in crystalline solids", Monograph No. 33 (Institute of Metals, London, 1969) p. 59.
12. W. JOHNSON and R. MEHL, *Trans. Met. Soc. AIME* **135** (1939) 416.
13. J. W. CHRISTIAN, "The theory of transformations in metals and alloys" (Pergamon Press, Oxford, 1965).
14. F. S. HAM, *J. Appl. Phys.* **30** (1959) 1518.

Received 29 October and accepted 31 December 1974.